Available online at www.sciencedirect.com
ScienceDirect
Trans. Nonferrous Met. Soc. China 29(2019) 1842−1853
Transactions of Nonferrous Metals Society of China
www.tnmsc.cn

Effects of solution treatment on high temperature deformation behavior of extruded Mg−0.35Y−2.17Nd−0.36Zr biomedical alloy

Sh. ALIYARI, S. M. FATEMI, S. M. MIRESMAEILI

Department of Metallurgy and Materials Engineering, Shahid Rajaee Teacher Training University, P. O. Box 136-16785, Tehran, Iran

Received 30 January 2019; accepted 21 June 2019

Abstract: The high temperature deformation behavior of an extruded Mg−0.35Y−2.17Nd−0.36Zr (wt.%) alloy was investigated for biomedical application by employing compression tests in temperature range of 225−525 °C and strain rate range of 0.0003−0.03 s^{-1}. To study the significance of solute elements, the material was solution-treated before deformation. The low temperature yield strength of the as-extruded material significantly decreased after solutionizing process. A drastic change in the strength of solutionized alloy was recorded as the temperature was raised to 450 °C, which was attributed to the promotion of grain boundary sliding (GBS). It was evidently shown that the slip-to-twinning transition temperature did not necessarily coincide with the strength-drop temperature. Based on constitutive equations, deformation parameters and related activation energy for the experimental alloy have been determined, incorporating the strain-dependent material constants. The verification of predictability of the developed models indicates a good agreement between experimental and predicted data.
Key words: Mg alloy; hot deformation; constitutive model; twinning

1 Introduction

In recent years, magnesium alloys containing rare earth (RE) elements have attracted the interest of researchers as biodegradable materials for medical devices. Proper results were reported for their in vitro [1] and in vivo [2] performance to assess the potential of using these materials as realistic alternatives for permanent implants. In addition to potential cardiovascular applications, magnesium alloys were addressed to be applied as lightweight, biodegradable, load-bearing orthopedic implants for possible substitution of natural tissue [3]. From this class of materials, Mg−Y−RE−Zr (WE43) alloy has reached an industrialization potentials on the basis of desired corrosion behavior [4] as well as clinical pilot results [5].

To achieve reasonable mechanical properties for the medical devices, the feedstock material for industrial manufacturing must be processed through operations involving high-temperature deformation. Accordingly, the processing parameters should be compromised to control the microstructure evolutions, and thereby the final mechanical properties of the material. It has been realized that the addition of rare earth (RE) elements can either lead to randomization of crystallographic texture [6,7], or constitute high temperature-resistant precipitates within magnesium matrix [8,9]. For example, a texture weakening could be achieved by hot extrusion, multi-pass rolling and plane strain compression in the presence of RE elements [9,10]. Moreover, by addition of RE elements, strength of magnesium alloys increases due to precipitation hardening and solid solution strengthening mechanisms [11,12].

Knowledge with regard to the deformation behavior of Mg−RE alloys is complicated by many possible combinations of deformation mechanisms such as twinning−slip activities, texture weakening, solute and precipitation hardening, the contribution of which is dictated by processing parameters such as temperature and strain rate. To exploit the benefits of these magnesium alloys, it is crucial to recognize material behavior under specified deformation conditions and also to increase the limited available flow stress data.

Numerous researches could be found in the literature dealing with the high temperature deformation behavior of RE containing magnesium alloys. YANG et al [13] analyzed plastic deformation and dynamic

Corresponding author: S. M. FATEMI; Tel/Fax: +98-21-22970047; E-mail: mfatemi@sru.ac.ir
DOI: 10.1016/S1003-6326(19)65092-2

recrystallization (DRX) behavior of Mg−5Gd−4Y−0.5Zn−0.5Zr alloy. They mainly concerned with the development of flow rule of alloy and a new method to quantify the progress of DRX in metals using stress−strain curves. The hot working behavior of Mg−Gd−Y−Nb−Zr alloy was also recently investigated using constitutive model, where processing maps were constructed at different strains for Mg−Gd−Y−Nb−Zr alloy based on dynamic materials model [14]. Also, a study on deformation behavior of a cast Mg−7Gd−5Y−1.2Nd−Zr showed that the flow stress of magnesium alloy during high temperature deformation can be represented by a Zener−Hollomon parameter in the hyperbolic Arrhenius-type equation [15]. Even though there are more studies in the case of Mg−Gd alloys, fewer researches focused on the response of Mg−Y alloys to hot deformation. AZZEDINE and BRADAI [16] have reported serrated flow during deformation of Mg−Y−Nd−Zr (WE54) alloy at 300 and 400 °C, which was attributed to the strong interaction of Y and Nd with dislocations. BELADI and BARNETT [17] studied the effects of aging pre-treatment at 170, 250 and 300 °C on the compressive deformation of an as-cast WE54 alloy. They showed that the work hardening behavior of the material changed with increasing temperature depending on the pre-aging condition. The compressive flow behavior of as-cast WE43 magnesium alloy at high temperatures and strain rates of 0.01, 0.1, 0.5 and 1 s^{-1}, was investigated by GAO et al [18], where a heat activation energy of 297 kJ/mol was determined for deformation.

Summarizing the reported researches implied that there are inadequate data available on the deformation behavior of wrought Mg−Y−Nd−Zr alloys, whereas most of present investigations have started with alloys containing different (Mg,RE) second phases [19,20]. Moreover, the individual influence of precipitates or solute elements on the flow stress behavior of RE-containing alloys has been insufficiently understood due to their indistinctive hardening effects on the material flow. Starting with a solutionized alloy provides a foundation for the study of flow behavior dominated by the RE-solute hardening effect. The study of solution-treated alloy in comparison to the precipitate-containing alloys assists to shed light on the isolated effect of RE solute elements on the deformation behavior as well as microstructural behavior of WE alloy. Accordingly, in this research, the deformation behavior of a solutionized wrought (Mg−Y−Nd−Zr) WE43 alloy has been experimentally studied using isothermal hot compression tests in a wide temperature range of 225−525 °C under different strain rates. The obtained data assisted to derive constitutive equations relating flow stress, strain rate and temperature considering a proper compensation of strain.

2 Experimental

An extruded WE43 magnesium alloy (Mg−4.35Y−2.17Nd−0.36Zr, wt.%) with 60 mm in diameter was received as the experimental material in this research, the microstructure of which was presented in Fig. 1. X-ray diffraction data, shown in Fig. 1(b), confirmed that the initial microstructure contained $Mg_{24}Y_5$ eutectic phase. The material was solutionized at 480 °C for 3 h to dissolve precipitates as well as eutectic phase. The optical micrograph of the solutionized alloy was depicted in Fig. 1(c), where the precipitates disappeared. The mean grain size was measured to be 70 μm.

The cylindrical compression testing specimens were machined with diameter of 8 mm and height of 12 mm,

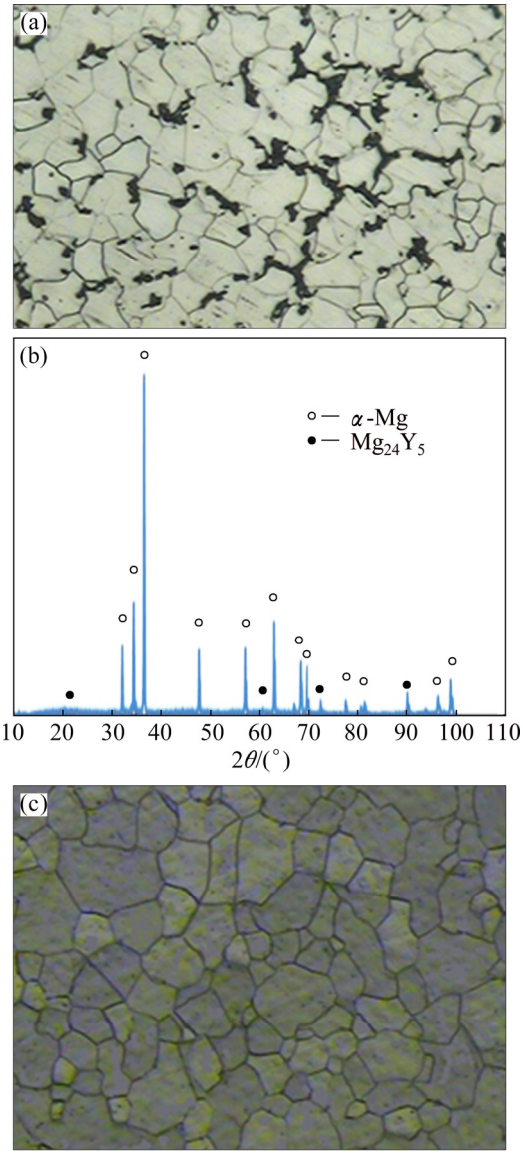

Fig. 1 Optical microstructure (a), X-ray diffraction pattern (b) of as-received extruded WE43 alloy and optical microstructure of experimental material in solutionized conditions (c)

where the compression axis was selected to be parallel to the prior extrusion direction. The hot compression experiments were performed using GOTECH A17000 universal testing machine equipped with programmable resistance furnace. The thin mica plates were used to reduce the friction effect between the specimens and the anvils. Prior to the test, the specimens were soaked at the predetermined deformation temperature for 7 min to equilibrate the temperature throughout the specimens. The experiments were conducted in the temperature range of 225−525 °C with 75 °C intervals under strain rates of 0.0003, 0.003 and 0.03 s^{-1}. As deformation behavior and related mechanism were reported, in common magnesium alloys, that the microstructure started to change around 225−250 °C, 225 °C is considered as the lowest working temperature. Moreover, as the WE alloys are supposed to possess superior high temperature mechanical properties, a temperature as high as 525 °C was selected as the maximum temperature. Each compression test was repeated at least three times with three different samples. To compare the yield strengths, the compression tests were also conducted for the as-extruded material (with no solutionizing treatment) at 0.0003 s^{-1}. The specimens were hot compressed up to the strain of 0.6 followed by quenching in water right after straining. The deformed specimens were sectioned parallel to the compression axis. The samples for SEM experiments were ground, polished and etched using acetic picral solution. The EBSD of twin bands was performed using scanning electron microscope (FEGeSEM, Zeiss Ultra Plus) coupled with energy dispersive spectroscope (EDS). X-ray dot maps were used to analyze the segregation of RE elements. In order to perform TEM investigation of the deformed material, slices of the compressed sample was first cut parallel to the compression direction, and then thinned by grinding to a sheet with 100 mm in thickness. A disc with 3 mm in diameter was subsequently punched out from the sheet, ensuring that the targeted area was located close to the center of the disc. The TEM thin foils were prepared by a twin-jet polishing technique. The perforation was done by a solution of 1% perchloric acid, 99% ethanol at a polishing temperature of −30 °C.

3 Result and discussion

3.1 Flow stress behavior

True stress−true strain curves obtained from the compression tests at different temperatures and strain rates are presented in Fig. 2. As is seen, the flow stress is initially increased with strain up to a peak stress (corresponding to ε_P) and then decreased by a rate that decays with increasing strain. It is obvious that with increasing strain rate and decreasing temperature the

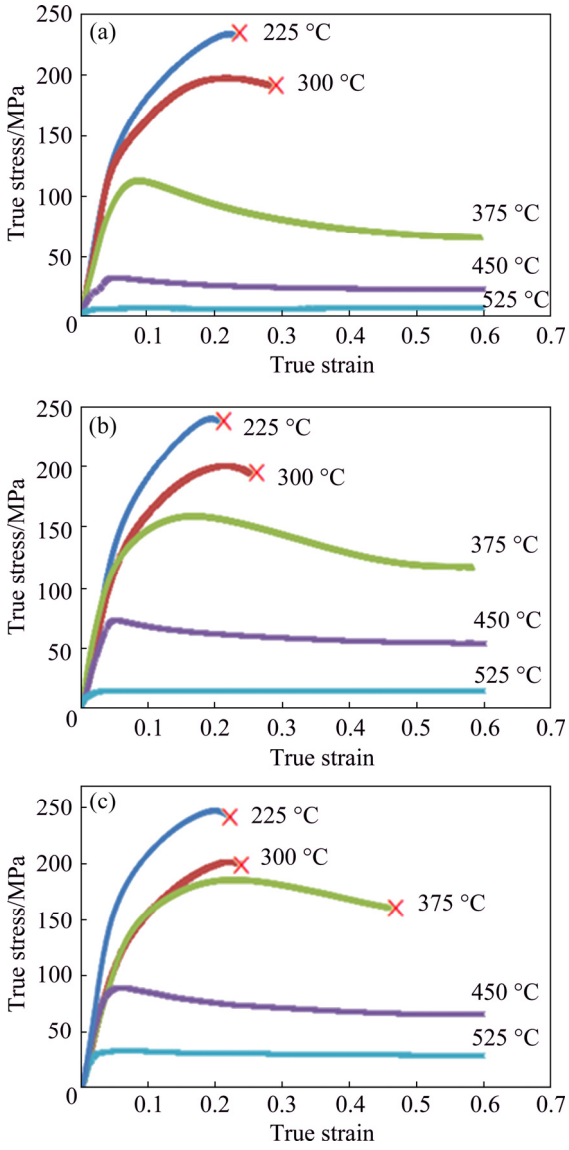

Fig. 2 True stress−true strain behavior of experimental alloy obtained by hot compression tests at different strain rates: (a) 0.0003 s^{-1}; (b) 0.003 s^{-1}; (c) 0.03 s^{-1} [20]

flow stresses shift to higher levels, though the strain hardening and softening rates are varied with deformation temperature and strain rate. As the temperature increased and strain rate decreased, lower hardening rate appeared at low strains so that lower values for peak strain, peak and steady state stresses were recorded. The latter observations are commonly related to thermally-activated recovery process which itself is governed by atomic diffusion. Thus, higher temperatures and lower strain rates (longer time for diffusion) may result in a lower hardening rate. The authors believe that the observed work softening may be related to the depletion of alloying element particularly the Y atoms from the solid solution. Similar explanation was given for the precipitation-hardened alloy [8]. Solute

atoms may be drawn toward deformation dislocations as a result of the interactions of their strain fields, and eventually concentrate around dislocations. If the solute atoms have a mutual attraction, the precipitation of a second crystalline phase may start at dislocations. When the solute atoms do not combine to form a new phase, an equilibrium state should develop, where a steady-state concentration of solute atoms builds up around the dislocation which is higher than that of the surrounding lattice. This is the case which was traced during deformation of the experimental alloys (Fig. 3), where the segregation of alloying atoms led to the formation of dislocation networks after deformation to true strain of 0.4 at 400 °C. The segregation of alloying atoms was observed in the microstructure deformed up to higher strains, which is typically depicted using SEM−EDS micrograph in Fig. 4, revealing the areas enriched in Y and Nd elements after deformation to a strain of 0.4 at 375 °C. Our systematic research aiming to precisely-study this notion is underway. As is observed, at strain rate of 0.0003 and 0.003 s^{-1} premature fracture at low strains occurred at 225 and 300 °C. As the strain rate was increased to 0.03 s^{-1}, premature fracture was observed even at high temperature of 375 °C. The latter can be explained by higher hardening rate of material at high strain rate, where the applied deformation rate could not be accommodated by material hardenability provided by basal slip as well as limited non-basal slip activities. However, at higher temperatures, deformation continued up to the strain of 0.6.

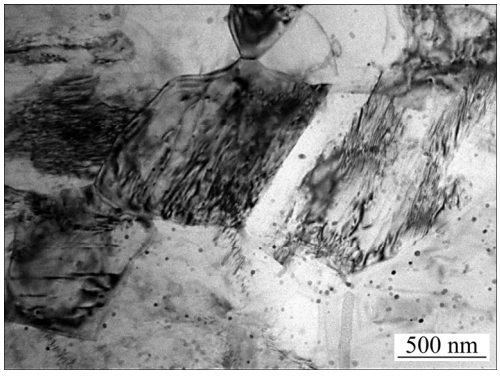

Fig. 3 TEM micrograph showing dislocation network in experimental alloy deformed to strain of 0.4 at 400 °C

The yield strength values obtained for solutionized material at different temperatures, as well as those for the as-extruded material (without solutionizing) are shown in Fig. 5. It is apparent that the low temperature (below 400 °C) yield strength of the as-extruded material significantly decreases after solutionizing heat treatment. Thus, higher strength of as-extruded alloy may be rationalized in terms of the dominated activity of basal slip at low temperatures. Crystal plasticity modeling

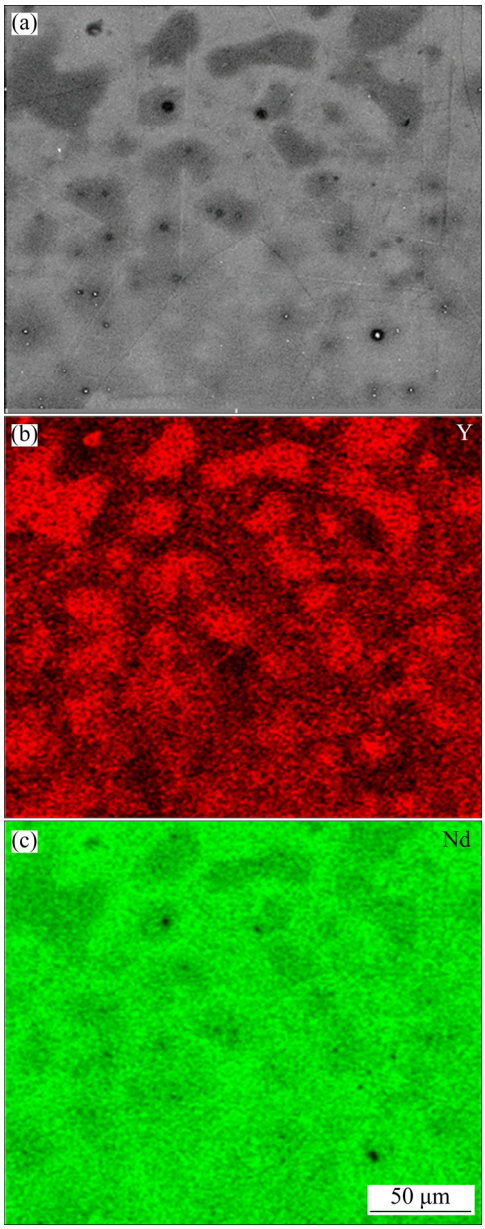

Fig. 4 SEM micrograph (a) and EDS dot maps of Y (b) and Nd (c) elements of experimental alloy deformed to strain of 0.4 at 375 °C and 0.003 s^{-1}

results reported by AGNEW et al [21], revealed that the basal slip mode in Mg−RE alloy may be significantly strengthened by the presence of second phase particles. However, solutionized alloy exhibit higher strength as the temperature raised to 450 and 525 °C. This is a surprising result, as the WE43 alloy is considered as a precipitation-hardened material with high temperature service performance. NIE [22] predicted that the critical stress for non-basal slips is not strongly altered by the precipitates. Thus, if one considers the level of strengthening achieved due to increased solute atoms in the matrix, the net influence due to solutionizing of $Mg_{24}Y_5$ precipitates would be expected to be alloy

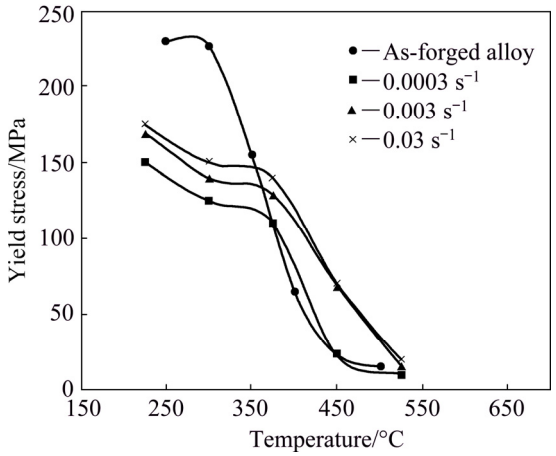

Fig. 5 Variation of yield strength with temperature in different strain rates of solutionized alloy (present study) and as-forged alloy of same alloy

strengthening. In support of this speculation, previous results showed that yttrium and neodymium are very effective solid solution strengthener in magnesium due to size and/or modulus misfits between solute and solvent atoms and also the valency effect [23]. They were found to give a considerably abnormal higher strengthening effect than Al and Zn. Present results also validate the previously reported results that the Mg24Y5 eutectic particles take a minor role in high temperature strength of the WE43 alloy [22], where plate-shaped β phase is considered to be the key strengthening constituent.

The evolution of yield strength data obtained for the solutionized material at different strain rates (Fig. 5) indicates a low-rate decrease from 225 to 375 °C. The softening mechanisms based on atomic diffusion could monotonically reduce the yield strength of the materials with increasing temperature. However, as the temperature raised to 450 °C, a drastic change in strength was recorded. In contrast, for the as-extruded experimental alloy, the significant decrease in yield strength is observed at 350 °C, which is in agreement with previous results, denoting that WE43 alloy preserves the strength up to 300 °C [24]. It is interesting to note that the solutionizing treatment of the experimental alloy resulted in an increase in strength-drop temperature. Accordingly, a change in deformation mechanisms is assumed to be responsible for the strength-drop observed for the solutionized material at 450 °C. As dislocation motion may be restricted by misfit-stress field of Y and Nd atoms [25], it is likely that deformation at 450 and 525 °C may be associated with inhomogeneous plasticity and thereby accelerated dynamic recovery in the grain boundary regions. In such circumstances, grain boundary sliding (GBS) may be involved [26], taking an effective role to rapidly decrease the yield strength. Consistently, the occurrence of GBS was reported in Mg−Y−RE alloy in temperature range of 430−475 °C [20]. The higher strength-drop for the solutionized alloy suggests that solute RE elements may limit the extent of GBS activity and preserve the strength more effectively than that the RE-containing precipitates do in the as-extruded alloy. The RE elements impose their influence through slowing down the movement of GB and introducing a strong GB pinning effect, owing to the GB segregation and their slow diffusivity in Mg [20].

Figure 6 indicates the variation of peak stress versus $1/T$, for the three experimental strain rates. As is observed, the data fitted in two linear behaviors for all three strain rates. The slop-change, i.e., the drop in peak stress, appears with increasing temperature to 450 °C. Some previous researches claimed that the changes in flow stress of Y/RE-containing magnesium alloys with ascending temperature ("high temperature behavior") is related to the cessation of twinning and transition to slip dominant deformation [17]. To testify this opinion in the present work, some compressive tests were interrupted at strain of 0.2, and the samples were immediately quenched in water to preserve the developed microstructure. The microstructural results obtained at strain rate of 0.003 s^{-1} and different temperatures are typically given in Fig. 7. It is obvious that twinning contributed during deformation at 225 and 300 °C, while it reached to a diminishing degree as the temperature was raised to 375 °C. Misorientation analysis of the electron back scattered diffraction (EBSD) results, given in Fig. 8, determined that the twins are of "extension" type. Thus, 375 °C is identified as the transition temperature for twinning-to-slip dominated flow. Therefore, it is revealed that the slip-to-twinning transition temperature (375 °C) does not necessarily coincide with the strength-drop temperature (450 °C); the former is reflective of the operation of non-basal slip, while the latter possibly denotes the temperature at which GBS is promoted, referring the discussion given in the above paragraph.

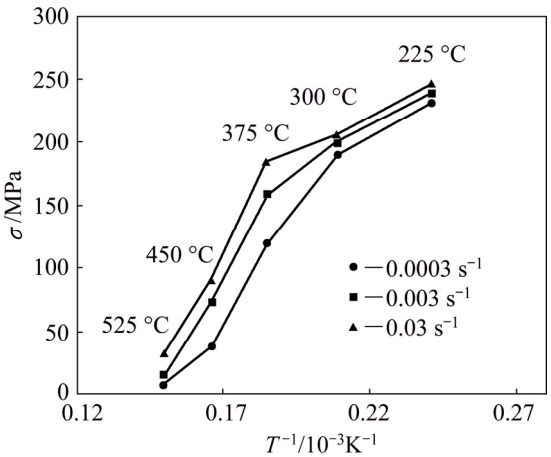

Fig. 6 Variations of peak stress with temperature at different strain rates

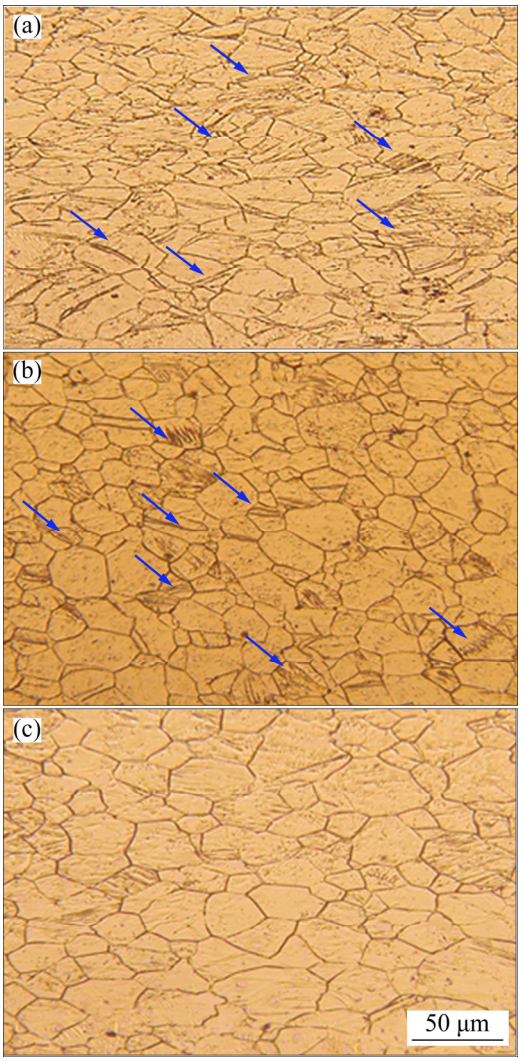

Fig. 7 Optical microstructures of compression specimens at strain of 0.2 and different temperatures of 225 °C (a), 300 °C (b) and 375 °C (c), deformed under constant strain rate of 0.003 s^{-1} (twins are typically arrowed)

The twinning-to-slip transition temperature obtained for the experimental alloy is higher than that reported for the AZ grades [27]. Similar phenomenon was previously assessed by BELADI and BARNETT [17] in WE54 alloy, though no enough explanation was given to justify the observation. RE elements harden all the slip systems in magnesium alloys due to their different atomic sizes and low diffusivity [25]. Once the dragging effect of RE hinders basal slip in the early stage of deformation, the non-basal slip and twinning should be activated. Moreover, as RE elements effectively reduce the stacking fault energy [28], the cross slip of screw dislocations from basal to non-basal plane is retarded. Accordingly, the occurrence of twinning may be promoted in an extended temperature range, leading to a higher twinning-to-slip transition temperature. As the temperature is sufficiently raised, the diffusivity of RE elements increases and thereby the activation energy for prevalence of non-basal slip is reached.

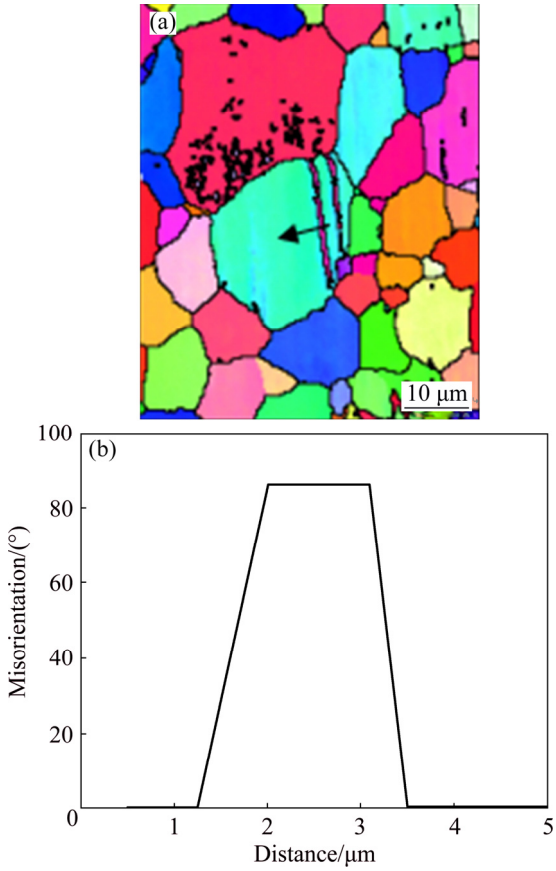

Fig. 8 EBSD map of experimental alloy including twins forming during deformation at 300 °C (a) and misorientation profile across twin (b) arrowed in (a)

The aforementioned explanations are based on the RE elements in dissolved state. RE elements in solutionized Mg−Y−Nd−Zr alloys may harden the basal slip much more than prismatic slip, stimulating the material to deform through twinning rather than non-basal slip [29]. Furthermore, dissolved RE elements may facilitate twinning through formation of short range order regions. The higher transition temperature may be also eminent in the as-extruded alloy containing precipitates. The critical stress for twinning is not strongly altered by the aging treatments [21], while precipitates in the Mg matrix and GBs can restrict dislocation and GB mobility (pinning effect) during deformation [20], thereby a slight increase in the slip-to-twinning transition temperature maybe expected even in the precipitate-containing alloys. The latter effects may rationalize a further increase in transition temperature in solutionized alloys rather that aged ones. This elucidation justified the results reported by BELADI and BARENET [17], and AGNEW and DUYGULU [30] where a higher transition temperature was reported under solutionized condition.

3.2. Constitutive equation

The hyperbolic sine-type equation has been extensively employed to characterize the relationship among flow stress (σ), temperature (T) and strain rate ($\dot{\varepsilon}$) in a broad range of stresses [31,32]:

$$\dot{\varepsilon}=A[\sinh(\alpha\sigma)]^n\exp[-Q/(RT)] \quad (1)$$

where Q is the activation energy (J/mol), R is the universal gas constant (8.314 J·mol^{-1}·°C^{-1}), and A (s^{-1}), α (MPa^{-1}) and n are material constants.

The value of α is derived by dividing β by n_1 ($1/n_1=m$). These two material constants, β and n_1, are obtained through taking the logarithm from exponential law and power law constitutive equation (Eqs. (2) and (3)) and determining the slope values of $\ln\sigma$ vs $\ln\dot{\varepsilon}$ and σ vs $\ln\dot{\varepsilon}$ plots, respectively (Fig. 9).

$$\ln\sigma=\frac{1}{n_1}\ln\dot{\varepsilon}-\frac{1}{n_1}\ln B \quad (2)$$

$$\sigma=\frac{1}{\beta}\ln\dot{\varepsilon}-\frac{1}{\beta}\ln C \quad (3)$$

where B and C are constants [33]. At 225 and 300 °C, an almost zero sensitivity was measured. This is consistent with the high transition temperature of the present alloy and prevalence of twinning during deformation at 225 and 300 °C. However, this is in contrast to the data reported for AZ grades; for instance, the strain rate sensitivity increases from 0.01 to 0.15 between room temperature and 200 °C for AZ31 alloy [30].

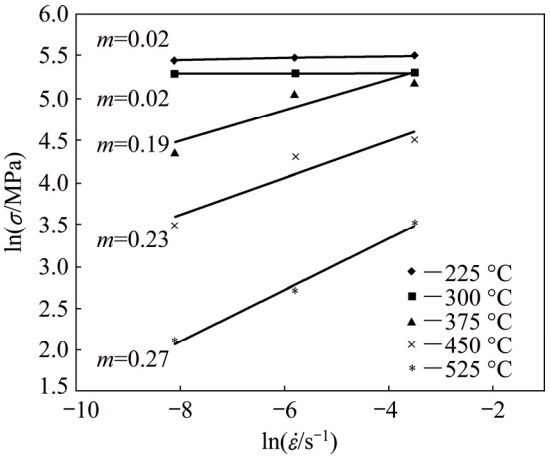

Fig. 9 Variations of peak stress with strain rate for experimental alloy according to power law

At temperatures equal and above 375 °C, the value of m increases, which represents change in the deformation mechanism from twinning to slip, as also illustrated in Fig. 9.

Due to the large difference in the values of n_1, between two low temperatures and higher temperatures in peak strain, the rest of the data modeling and calculation of the activation energy is done only for data belonging to three higher temperatures and strain of 0.45. At this strain, relatively enough time may be provided to overcome the hardening mechanisms and achieve steady state stresses for all deformation conditions. Figure 10 displays the evolution of flow stress at strain of 0.45, in according to both power and exponential laws. According to Eqs. (2) and (3), the mean value of n_1 and β are determined to be 3.70 and 0.077, respectively. Therefore, the value of α is derived to be 0.021 MPa^{-1}.

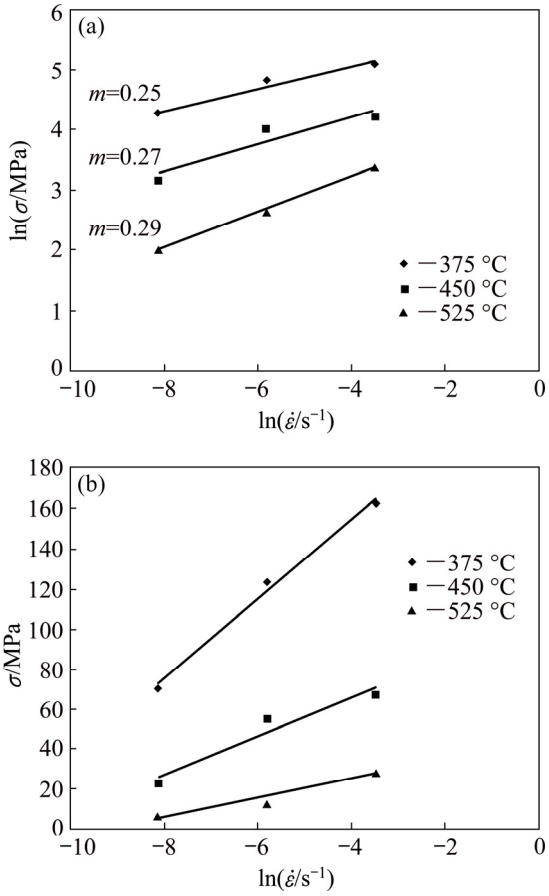

Fig. 10 Variations of flow stress with strain rate for experimental alloy at true strain of 0.45 according to power law (a) and exponential law (b)

The value of n is determined by taking the logarithm of both sides of Eq. (1):

$$\ln[\sinh(\alpha\sigma)]=\frac{\ln\dot{\varepsilon}}{n}+\frac{Q}{nRT}+\frac{\ln A}{n} \quad (4)$$

And at a constant strain rate, the partial differentiating Eq.(1) gives

$$Q=Rn\frac{\mathrm{d}\ln[\sinh(\sigma\alpha)]}{\mathrm{d}(1/T)} \quad (5)$$

Thus, the average slopes of the lines by plotting $\ln[\sinh(\alpha\sigma)]$ versus $\ln\dot{\varepsilon}$, in Fig. 11(a), would give the n-value. The Q parameter also is determined from the slope of $\ln[\sinh(\alpha\sigma)]$ versus $1/T$ (Fig. 11(b)), and

applying the n-value to Eq. (5). The activation energy is obtained to be 247.78 kJ/mol, approximately for the given strain. This value is lower than that reported for as-cast WE43 alloy in compression test and strain rate of 0.01−1 s^{-1} by GAO et al (i.e., 297.15 kJ/mol) [18]. This discrepancy in Q values may be attributed to the difference in deformation regime and also the condition of initial materials. AZZADINE and BRADAI [16] indicated that the activation energy (Q) depends strongly on the deformation conditions (temperature and strain rate). For example, for alloys of Mg−Ce−Zn−Zr and Mg−Y−Nd−Zr at constant temperature, by increasing strain rate of deformation, the values of Q determined increase.

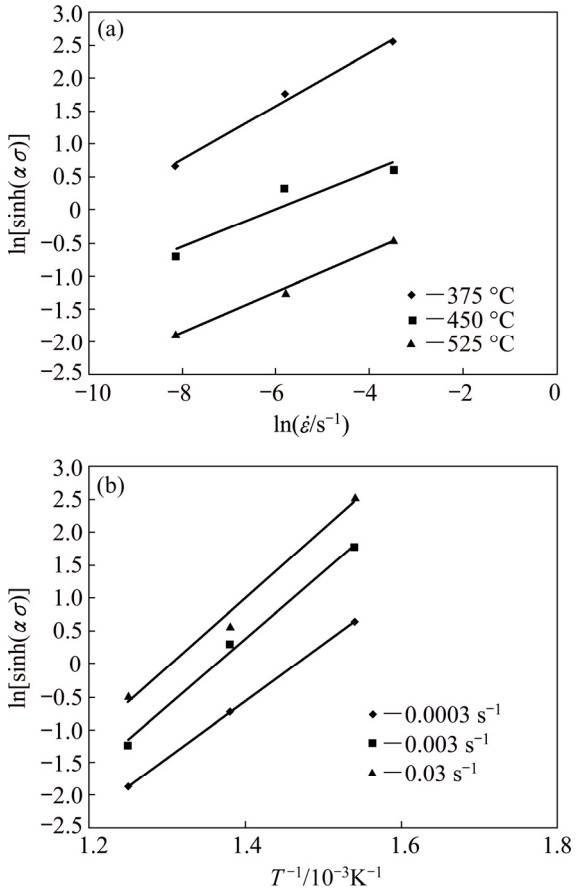

Fig. 11 Variations of ln[sinh($\alpha\sigma$)] with $\ln\dot{\varepsilon}$ (a) and 1/T (b), at true strain of 0.45 and different temperatures, by assuming α=0.021 MPa^{-1}

Previous researches have reported, in comparison to the present data, remarkably lower activation energy at similar deformation conditions for classic magnesium alloys. For example, 180.9 and 164 kJ/mol have been determined for AZ81 and AZ31 magnesium alloy, respectively. This disparity, at least partly, may be explained considering low diffusivity of RE elements compared to Al and Zn in Mg as well as solute dragging effect of REs with large difference in atomic radius with magnesium. GUO et al [34] suggested that the stronger Mg−Y atomic bond compared to Mg−Al may intensify the latter effects. The high activation energy of 247.78 kJ/mol assessed for higher temperatures, is close to 230 kJ/mol reported for the creep of a WE43 alloy in the same temperature regime [35]. An activation energy of 230−290 kJ/mol was also achieved for binary Mg−(0.7−3.9)Y alloys crept at temperature between 277 and 377 °C [11].

To find the rate-controlling mechanisms during hot deformation, the values of Q and n obtained from hyperbolic sine power law (Eq. (6)) constitutive equations may be reconsidered, which relates the Zener−Hollomen parameter (Z) to flow stress for a wide range of Z parameter [36]. Using Eq. (6), the correlation line is plotted in Fig. 12, the slop value of which is measured to be n=3.109.

$$Z=\dot{\varepsilon}\exp\left(\frac{Q}{RT}\right)=A[\sinh(\alpha\sigma)]^n \tag{6}$$

The obtained n value is consistent with the GBS as the rate-controlling mechanism, which suggests the stress exponent of 3, when the grain size is large. The occurrence of GBS should be accommodated by the movement of dislocations through slip within the adjacent grains [37]. As mentioned above, dragging effect of REs, makes dislocations slip difficult at the high experimental temperatures. On other hand, segregation of RE in GB may lead to more accumulation of dislocations and stress concentration at triple points and cause GBS to require higher activation energy [38]. The latter explanation may also rationalize the high value obtained for the experimental alloy. Accordingly, the hardened non-basal slip close to the grain boundaries which should accommodate the occurrence of GBS may be considered as the controlling deformation mechanism. Consistently, SUZUKI et al [11] discussed that the cross slip of basal dislocation from basal plane to prismatic

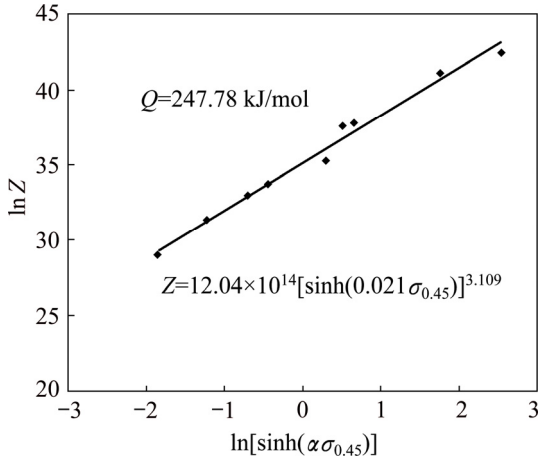

Fig. 12 Hyperbolic sine law analyses by consideration of $\sigma_{0.45}$ and Q=247.78 kJ/mol

plane of Mg matrix is associated with high activation energy in RE-containing alloys.

3.3 Compensation of strain

It is usually assumed that the influence of strain on flow stress behavior at evaluated temperature is insignificant and thereby would not be considered in Eq. (1) [39]. However, it has been recently shown in different studies, that material constants are influenced by the strain under hot deformation conditions [31]. Hence, compensation of strain should be taken into account to develop constitutive equation that predicts the flow stress. In order to incorporate the effect of strain in the constitutive equation, the values of material constants were evaluated at various strains (in range of 0.05−0.55) with an increment of 0.05 (Fig. 13). These values are polynomial functions of strains. The fifth order polynomial function is found to represent the strain effects on the material constants:

$$\begin{cases} n = A_0 + A_1\varepsilon + A_2\varepsilon_2 + A_3\varepsilon_3 + A_4\varepsilon_4 + A_5\varepsilon_5 \\ \alpha = B_0 + B_1\varepsilon + B_2\varepsilon_2 + B_3\varepsilon_3 + B_4\varepsilon_4 + B_5\varepsilon_5 \\ Q = C_0 + C_1\varepsilon + C_2\varepsilon_2 + C_3\varepsilon_3 + C_4\varepsilon_4 + C_5\varepsilon_5 \\ \ln A = D_0 + D_1\varepsilon + D_2\varepsilon_2 + D_3\varepsilon_3 + D_4\varepsilon_4 + D_5\varepsilon_5 \end{cases} \quad (7)$$

The coefficients of the fifth order polynomial functions are given in Table 1.

Table 1 Coefficients of polynomial functions for n, α, Q and $\ln A$

n coefficient	α coefficient	Q coefficient	$\ln A$ coefficient
A_0=0	B_0=0.0538	C_0=183.02	D_0=18.363
A_1=96.1	B_1=−0.599	C_1=4593.7	D_1=821.76
A_2=−853.37	B_2=3.9312	C_2=−43809	D_2=−7502.3
A_3=3251.1	B_3=−12.467	C_3=169831	D_3=28591
A_4=−5635.1	B_4=19.255	C_4=−297448	D_4=−49578
A_5=3653.7	B_5=−11.569	C_5=194501	D_5=32181

3.4 Verification of constitutive equation

To verify the developed constitutive equation, the experimental and predicted data were compared (Fig. 13). The flow stress can be predicted with calculated material constants at a particular strain, by reordering Eq. (1) and introducing the Zener−Holomen parameter ($Z=\dot{\varepsilon}\exp[Q/(RT)]$):

$$\sigma = \frac{1}{\alpha}\ln\left\{\left(\frac{Z}{A}\right)^{1/n} + \left[\left(\frac{Z}{A}\right)^{2/n} + 1\right]^{1/2}\right\} \quad (8)$$

As is seen in Fig. 14, a good agreement has been obtained between the experimental and predicted stress values.

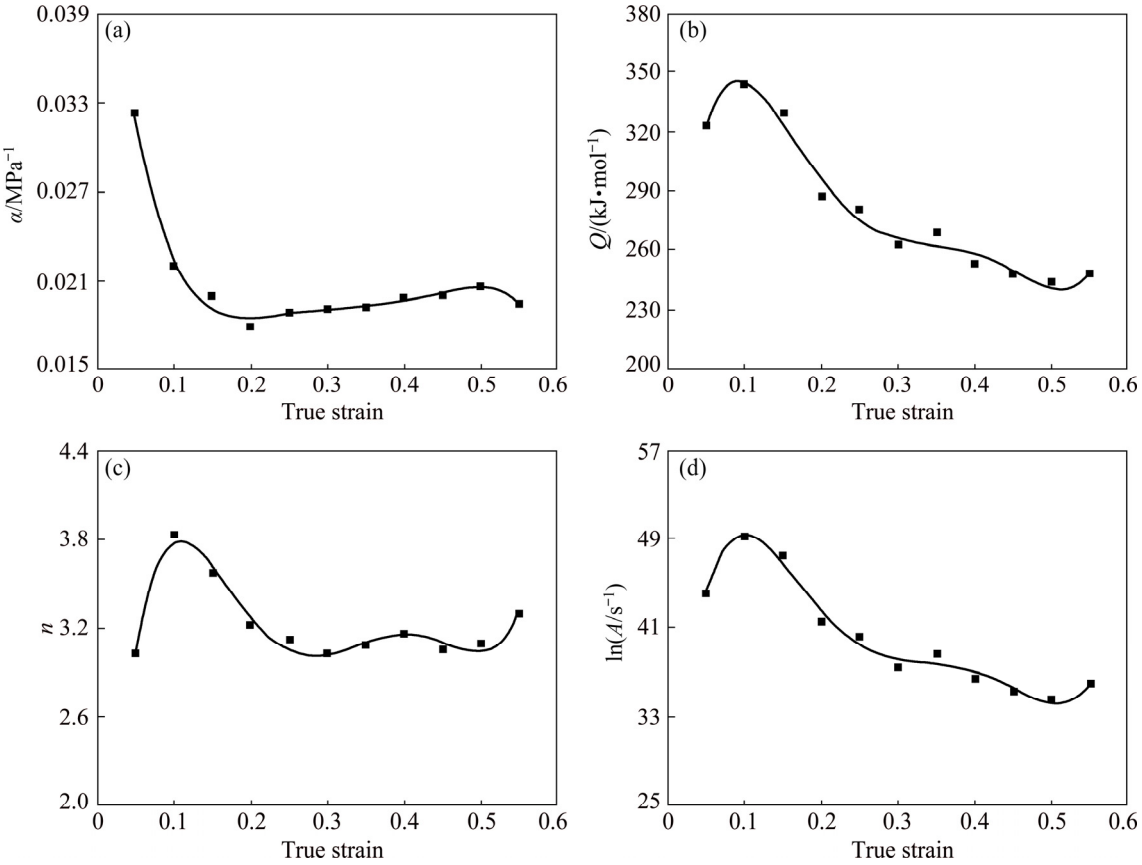

Fig. 13 Variations of α (a), Q (b), n (c) and $\ln A$ (d) with true strain based on fifth order polynomial-fit for WE43 experimental alloy

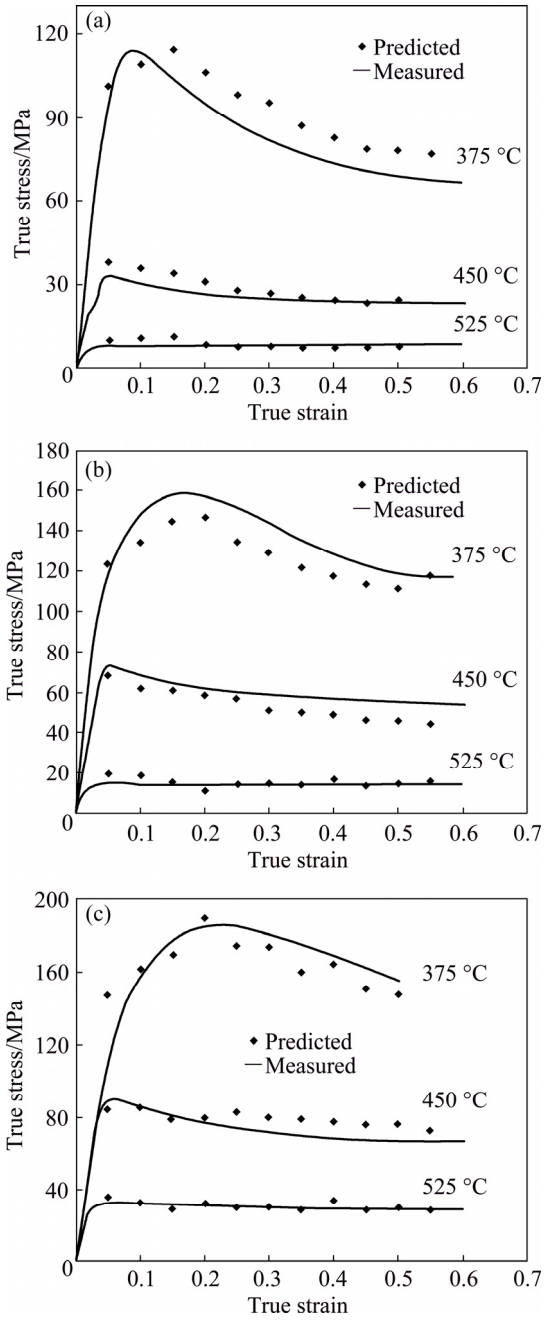

Fig. 14 Comparisons between predicted and measured flow stress curves of WE43 experimental alloy at different strain rates: (a) 0.001 s^{-1}; (b) 0.01 s^{-1}; (c) 0.1 s^{-1}

At the end, the predictability of the constitutive equation is quantified using standard statistical parameters such as correlation coefficient (R) and average absolute relative error (AARE, E_R). They are expressed as

$$R=\frac{\sum_{N}^{i=1}(E_i-\bar{E})(P_i-\bar{P})}{\sqrt{\sum_{N}^{i=1}(E_i-\bar{E})^2\sum_{N}^{i=1}(P_i-\bar{P})^2}} \quad (9)$$

$$E_R=\frac{1}{N}\sum_{i=1}^{N}\left|\frac{E_i-P_i}{E_i}\right|\times 100\% \quad (10)$$

where E is the experimental value and P is the predicted value from constitutive equation. $\bar{E}$ and $\bar{P}$ are the mean values of E and P, respectively. N is the total number of data. The correlation coefficient provides information about the strength of linear relationship between the experimental and predicted values (Fig. 15). The values of R and AARE were found to be 0.988 and 8.47%, respectively, which reflects the excellent predictability of the proposed constitutive model.

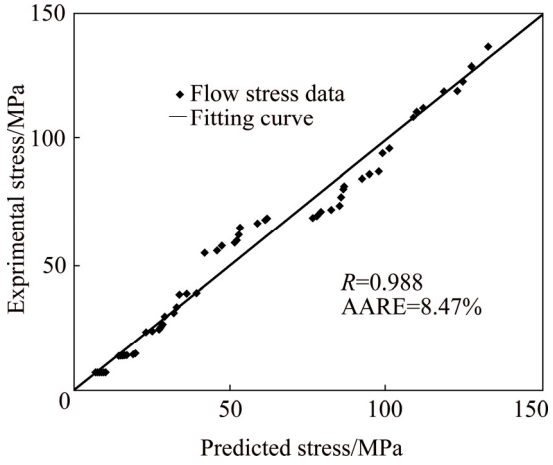

Fig. 15 Correlation between experimental flow stresses and predicted ones from proposed constitutive equation

Present results pointed out that, comparable to the Orowan hardening of the precipitates, the RE elements may provide high temperature strength for the experimental magnesium alloy even in the dissolved state. This finding was discussed relying on their effect on the SFE, basal and non-basal dislocation pinning and formation of short range order regions. Moreover, a high temperature strength-drop was realized at 450 °C, which was related to the operation of GBS. In spite of the changes in the deformation mechanism, the flow behavior of the experimental alloy could be convincingly modeled using strain-compensated constitutive equation.

4 Conclusions

(1) A strength-drop is realized at 450 °C, which is attributed to the promotion of GBS.

(2) The twinning-to-slip transition temperature of 375 °C was measured for the experimental alloy. It was concluded that the slip-to-twinning transition temperature does not necessarily coincide with the strength-drop temperature.

(3) The higher transition temperature in the RE-containing alloys was discussed considering different strengthening effects of RE elements on twinning and

slip systems.

(4) It was suggested that RE elements may further increase the transition temperature of magnesium alloy in the dissolved state than in aged condition.

(5) The constitutive equations have been proposed to correlate deformation parameters. The activation energy of deformation for the experimental alloy was determined.

(6) The material constants of constitutive equations have been found to be dependent on strain in function of the fifth order polynomial.

(7) The verification of predictability of the developed models indicates that a good agreement between experimental and predicted data has been established.

References

[1] SMOLA B, JOSKA L, BŘEZINA V, STULÍKOVÁ I, HNILICA F. Microstructure, corrosion resistance and cytocompatibility of Mg−5Y−4Rare Earth−0.5 Zr (WE54) alloy [J]. Materials Science and Engineering C, 2012, 32: 659−664.

[2] O'BRIEN B, CARROLL W. The evolution of cardiovascular stent materials and surfaces in response to clinical drivers: A review [J]. Acta Biomaterialia, 2009, 5: 945−958.

[3] STAIGER M P, PIETAK A M, HUADMAI J, DIAS G. Magnesium and its alloys as orthopedic biomaterials: A review [J]. Biomaterials, 2006, 27: 1728−1734.

[4] NEUBERT V, STULÍKOVÁ I, SMOLA B, MORDIKE B, VLACH M, BAKKAR A, PELCOVÁ J. Thermal stability and corrosion behaviour of Mg−Y−Nd and Mg−Tb−Nd alloys [J]. Materials Science and Engineering A, 2007, 462: 329−333.

[5] WINDHAGEN H, RADTKE K, WEIZBAUER A, DIEKMANN J, NOLL Y, KREIMEYER U, SCHAVAN R, STUKENBORG-COLSMAN C, WAIZY H. Biodegradable magnesium-based screw clinically equivalent to titanium screw in hallux valgus surgery: Short term results of the first prospective, randomized, controlled clinical pilot study [J]. Biomedical Engineering Online, 2013, 12: 62.

[6] CHINO Y, SASSA K, MABUCHI M. Texture and stretch formability of a rolled Mg−Zn alloy containing dilute content of Y [J]. Materials Science and Engineering A, 2009, 513: 394−400.

[7] STANFORD N, ATWELL D, BEER A, DAVIES C, BARNETT M. Effect of microalloying with rare-earth elements on the texture of extruded magnesium-based alloys [J]. Scripta Materialia, 2008, 59: 772−775.

[8] ASQARDOUST S, ZAREI-HANZAKI A, FATEMI S, MORADJOY-HAMEDANI M. High temperature deformation behavior and microstructural evolutions of a high Zr containing WE magnesium alloy [J]. Journal of Alloys and Compounds, 2016, 669: 108−116.

[9] BRASZCZYŃSKA-MALIK K, GRZYBOWSKA A. Microstructure of Mg−5Al−0.4Mn−*x*RE (*x*=3 and 5 wt.%) alloys in as-cast conditions and after annealing [J]. Journal of Alloys and Compounds, 2016, 663: 172−179.

[10] HANTZSCHE K, BOHLEN J, WENDT J, KAINER K, YI S, LETZIG D. Effect of rare earth additions on microstructure and texture development of magnesium alloy sheets [J]. Scripta Materialia, 2010, 63: 725−730.

[11] SUZUKI M, SATO H, MARUYAMA K, OIKAWA H. Creep behavior and deformation microstructures of Mg−Y alloys at 550 K [J]. Materials Science and Engineering A, 1998, 252: 248−255.

[12] MARUYAMA K, SUZUKI M, SATO H. Creep strength of magnesium-based alloys [J]. Metallurgical and Materials Transactions A, 2002, 33: 875−882.

[13] YANG Z, GUO Y, LI J, HE F, XIA F, LIANG M. Plastic deformation and dynamic recrystallization behaviors of Mg−5Gd−4Y−0.5Zn−0.5Zr alloy [J]. Materials Science and Engineering A, 2008, 485: 487−491.

[14] ZHOU Z, FAN Q, XIA Z, HAO A, YANG W, JI W, CAO H. Constitutive relationship and hot processing maps of Mg−Gd−Y−Nb−Zr alloy [J]. Journal of Materials Science & Technology, 2017, 33: 637−644.

[15] MA Ming-long, ZHANG Kui, LI Xing-gang, LI Yong-jun, ZHANG Kang. Hot deformation behavior of rare earth magnesium alloy without pre-homogenization treatment [J]. Transactions of Nonferrous Metals Society of China, 2008, 18(S): s132−s139.

[16] AZZEDDINE H, BRADAI D. On some aspects of compressive properties and serrated flow in Mg−Y−Nd−Zr alloy [J]. Journal of Rare Earths, 2013, 31: 804−810.

[17] BELADI H, BARNETT M. Influence of aging pre-treatment on the compressive deformation of WE54 alloy [J]. Materials Science and Engineering A, 2007, 452: 306−312.

[18] GAO Jia-cheng, WANG Qiang, WANG Yong, LI Wei, NIU Wen-juan. Microstructure and kinetics of hot deformation WE43 magnesium alloy [J]. Rare Metals, 2008, 27: 405−409.

[19] KANDALAM S, SABAT R, BIBHANSHU N, AVADHANI G, KUMAR S, SUWAS S. Superplasticity in high temperature magnesium alloy WE43 [J]. Materials Science and Engineering A, 2017, 687: 85−92.

[20] FATEMI S M, ALIYARI Sh, MIRESMAEILI S M. Dynamic precipitation and dynamic recrystallization during hot deformation of a solutionized WE43 magnesium alloy [J]. Materials Science and Engineering A, 2019, 762: 138076−138087.

[21] AGNEW S, MULAY R, POLESAK F, CALHOUN C, BHATTACHARYYA J, CLAUSEN B. In situ neutron diffraction and polycrystal plasticity modeling of a Mg−Y−Nd−Zr alloy: Effects of precipitation on individual deformation mechanisms [J]. Acta Materialia, 2013, 61: 3769−3780.

[22] NIE J. Effects of precipitate shape and orientation on dispersion strengthening in magnesium alloys [J]. Scripta Materialia, 2003, 48: 1009−1015.

[23] GAO L, CHEN R, HAN E. Effects of rare-earth elements Gd and Y on the solid solution strengthening of Mg alloys [J]. Journal of Alloys and Compounds, 2009, 481: 379−384.

[24] MORDIKE B. Creep-resistant magnesium alloys [J]. Materials Science and Engineering A, 2002, 324: 103−112.

[25] JUNG I H, SANJARI M, KIM J, YUE S. Role of RE in the deformation and recrystallization of Mg alloy and a new alloy design concept for Mg−RE alloys [J]. Scripta Materialia, 2015, 102: 1−6.

[26] ROBSON J D, HAIGH S J, DAVIS B, GRIFFITHS D. Grain boundary segregation of rare-earth elements in magnesium alloys [J]. Metallurgical and Materials Transactions A, 2016, 47: 522−530.

[27] BARNETT M, KESHAVARZ Z, BEER A, ATWELL D. Influence of grain size on the compressive deformation of wrought Mg−3Al−1Zn [J]. Acta Materialia, 2004, 52: 5093−5103.

[28] SANDLÖBES S, FRIÁK M, ZAEFFERER S, DICK A, YI S, LETZIG D, PEI Z, ZHU L F, NEUGEBAUER J, RAABE D. The relation between ductility and stacking fault energies in Mg and Mg−Y alloys [J]. Acta Materialia, 2012, 60: 3011−3021.

[29] HIDALGO-MANRIQUE P, ROBSON J, PEREZ-PRADO M. Precipitation strengthening and reversed yield stress asymmetry in Mg alloys containing rare-earth elements: A quantitative study [J]. Acta Materialia, 2017, 124: 456−467.

[30] AGNEW S R, DUYGULU Ö. Plastic anisotropy and the role of non-basal slip in magnesium alloy AZ31B [J]. International Journal of Plasticity, 2005, 21: 1161−1193.

[31] LIN Y, CHEN X M. A critical review of experimental results and constitutive descriptions for metals and alloys in hot working [J]. Materials & Design, 2011, 32: 1733−1759.
[32] DENG J, LIN Y, LI S S, CHEN J, DING Y. Hot tensile deformation and fracture behaviors of AZ31 magnesium alloy [J]. Materials & Design, 2013, 49: 209−219.
[33] LIN Y, CHEN M S, ZHONG J. Constitutive modeling for elevated temperature flow behavior of 42CrMo steel [J]. Computational Materials Science, 2008, 42: 470−477.
[34] GUO Xu-tao, LI Pei-jie, ZENG Da-ben. Application of rare earth in heat resistant magnesium alloy [J]. Chinese Rare Earths, 2002, 32(2): 63−67. (in Chinese)
[35] WANG J, HSIUNG L, NIEH T, MABUCHI M. Creep of a heat treated Mg−4Y−3RE alloy [J]. Materials Science and Engineering A, 2001, 315: 81−88.
[36] MCQUEEN H J, RYAN N. Constitutive analysis in hot working [J]. Materials Science and Engineering A, 2002, 322: 43−63.
[37] WATANABE H, MUKAI T, KOHZU M, TANABE S, HIGASHI K. Effect of temperature and grain size on the dominant diffusion process for superplastic flow in an AZ61 magnesium alloy [J]. Acta Materialia, 1999, 47: 3753−3758.
[38] SOMEKAWA H, WATANABE H, MUKAI T. Effect of solute atoms on grain boundary sliding in magnesium alloys [J]. Philosophical Magazine, 2014, 94: 1345−1360.
[39] ASHTIANI H R, PARSA M, BISADI H. Constitutive equations for elevated temperature flow behavior of commercial purity aluminum [J]. Materials Science and Engineering A, 2012, 545: 61−67.

固溶处理对挤压 Mg−0.35Y−2.17Nd−0.36Zr 生物医用合金高温变形行为的影响

Sh. ALIYARI, S. M. FATEMI, S. M. MIRESMAEILI

Department of Metallurgy and Materials Engineering, Shahid Rajaee Teacher Training University, P.O. Box 136-16785, Tehran, Iran

摘　要：通过在 225~525 °C、应变速率 0.0003~0.03 s^{-1} 的条件下进行压缩试验，研究挤压 Mg−0.35Y−2.17Nd− 0.36Zr (质量分数%)生物医用合金的高温变形行为。为了研究溶质元素的影响，变形前对材料进行固溶处理。固溶处理后，挤压态材料的低温屈服强度明显降低。当温度升高到 450 ℃时，由于晶界滑移(GBS)的促进作用，固溶化合金的强度发生剧烈的变化。结果表明，滑移−孪生转变温度不一定与强度下降温度一致。在本构方程的基础上，结合与应变相关的材料常数，确定实验合金的变形参数和相应的活化能。对所建模型的可预测性进行验证，结果表明，实验数据与预测数据吻合较好。

关键词：Mg 合金；热变形；本构模型；孪生

(Edited by Bing YANG)